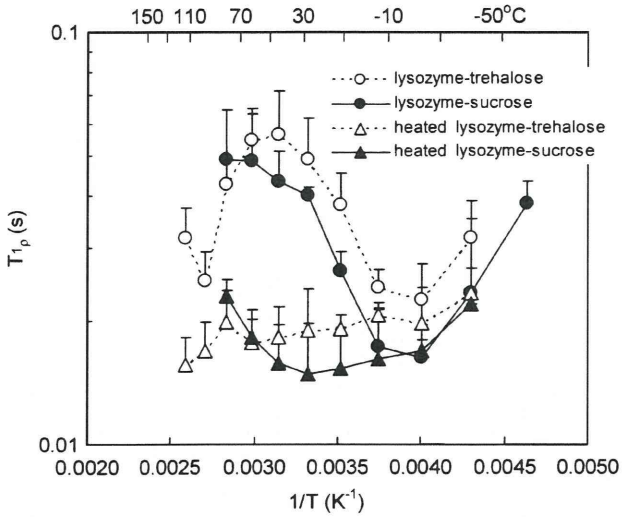

Fig. 5 Effect of heating on $T_{1\rho}$ of lysozyme carbonyl carbons in freeze-dried lysozyme-trehalose and lysozyme-sucrose. Heating was carried out at 62°C for 8 h. The error bars represent standard deviation ($n=3$).

the carbon has a single type of motion that shows a single τ_c.

$$\frac{1}{T_{1\rho}} = \frac{A\tau_c}{1+4\omega_1^2\tau_c^2} \tag{1}$$

where ω_1 is the strength of spin-locking and A is a constant determined by the gyromagnetic ratio of carbon, the number of protons involved in proton-carbon dipole interaction, which causes spin-lattice relaxation, and the distance between the carbon and the proton involved in the interaction. Because $T_{1\rho}$ becomes a minimum when $\tau_c = 1/2\omega_1$, the value of A can be determined from the

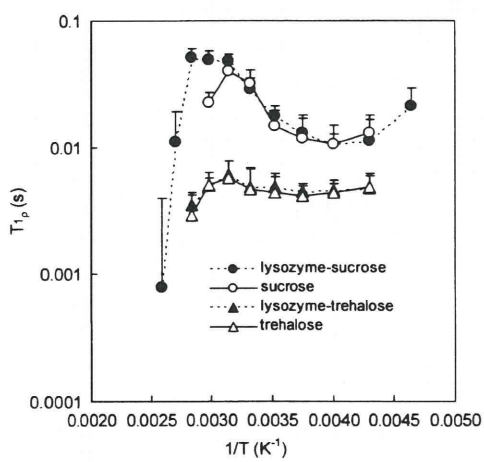

Fig. 6 Temperature dependence for $T_{1\rho}$ of carbons C-1 of trehalose and sucrose with and without lysozyme. The error bars represent standard deviation ($n=3$).

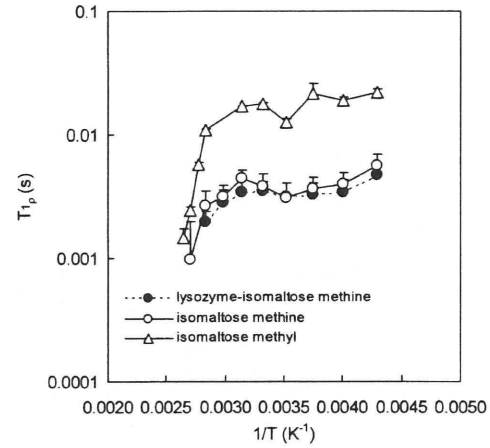

Fig. 7 Temperature dependence for $T_{1\rho}$ of carbon C-1 of isomaltose with and without lysozyme and temperature dependence for $T_{1\rho}$ of the methyl carbon of methylated isomaltose. The error bars represent standard deviation ($n=3$).

$T_{1\rho}$ value observed at the minimum ($T_{1\rho}$(min)) according to Eq. 2.

$$A = \frac{4\omega_1}{T_{1\rho}(\min)} \tag{2}$$

When the carbon has multiple types of motion with different τ_c values, $T_{1\rho}$ is described by an equation that sums the term for each τ_c value (Eq. 3).

$$\frac{1}{T_{1\rho}} = \sum_{i=1}^{n} \frac{A_i\tau_{c,i}}{1+4\omega_1^2\tau_{c,i}^2} \tag{3}$$

The analysis of NMR relaxation times using an equation comprising multiple terms of τ_c has been reported for the T_1 of ^2H of $[Co(H_2O)_6][SiF_6]$ (42) and the T_1 and $T_{1\rho}$ of ^{19}F for flufenamic acid dispersed in PVP (Aso *et al.*, unpublished data). The same approach can be applied to the $T_{1\rho}$ of the lysozyme carbonyl carbons (Fig. 3) by assuming that the carbon has two different types of molecular motion with different τ_c values and that each τ_c shows an Arrhenius type of temperature dependence (Eq. 4).

$$\tau_c = \tau_0 \exp\left(\frac{E_a}{RT}\right) \tag{4}$$

The regression curve obtained for each molecular motion is shown in Fig. 8a, and the temperature dependence of τ_c for each motion is compared in Fig. 8b, which also includes the temperature dependence of α-relaxation time as calculated by the Vogel-Tammann-Fulcher (385 kJ/mol) and the Adam-Gibbs-Vogel equations (29) (123 kJ/mol) at temperatures above and below T_g, respectively. The T_g and the fragility parameter were assumed to be 130°C and 50 (16), respectively. The two types of motion observed for the

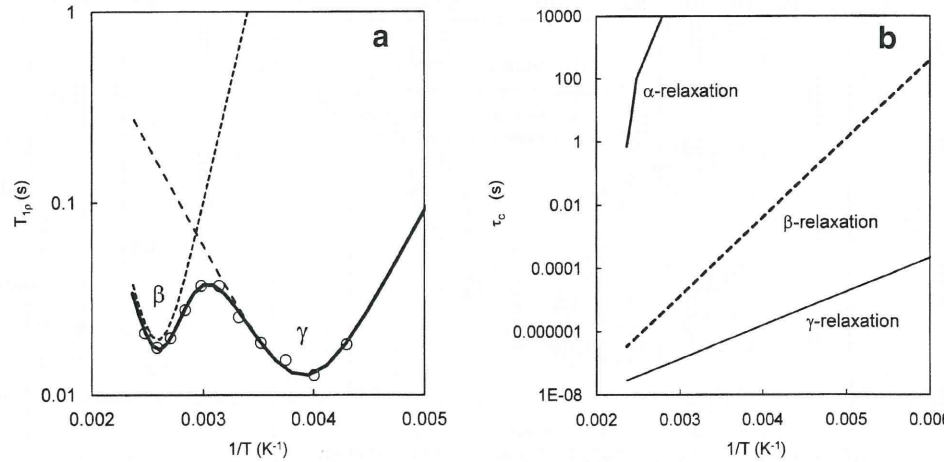

Fig. 8 (**a**) Regression curves for $T_{1\rho}$ of lysozyme carbonyl carbons in freeze-dried lysozyme obtained by assuming two different types of motion with different τ_c values. (**b**) Comparison of temperature coefficients of β- and γ-relaxation of lysozyme carbonyl carbons with that of α-relaxation time calculated assuming a T_g of 130°C and a fragility parameter of 50.

lysozyme carbonyl carbons revealed much smaller values of τ_c and Ea (i.e., slopes) than α-relaxation. The relaxation observed at higher temperatures showed a larger Ea and is referred to as β-relaxation in this paper. The other relaxation, observed at lower temperatures, is referred to as γ-relaxation. The parameters of $T_{1\rho}$(min), τ_0 and Ea were estimated to be 19 ms, 4×10^{-13} and 48 kJ/mol, respectively, for β-relaxation. For γ-relaxation, the parameters of $T_{1\rho}$ (min), τ_0 and Ea were estimated to be 13 ms, 9×10^{-11} and 20 kJ/mol, respectively.

The temperature dependence for the $T_{1\rho}$ of the lysozyme carbonyl carbons in the presence of sugars was also describable with a model that assumes that the carbon has two different types of molecular motion with different τ_c values, with each τ_c showing Arrhenius temperature dependence. The regression curves obtained for the freeze-dried lysozyme-trehalose, lysozyme-sucrose and lysozyme-isomaltose are shown in Fig. 9. The estimated parameters of $T_{1\rho}$(min) and Ea for β- and γ-relaxation are listed in Table I. The values of τ_c at 25°C calculated using these

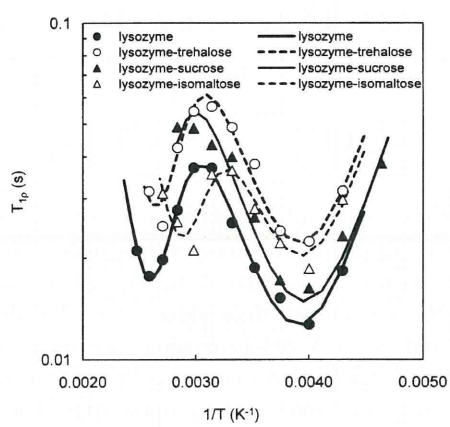

Fig. 9 Regression curves for $T_{1\rho}$ of lysozyme carbonyl carbons in lysozyme freeze-dried with sugars.

estimated parameters are also compared in Table I. The addition of sugars did not change the τ_c of the lysozyme carbonyl carbons or the Ea of τ_c for γ-relaxation. In contrast, τ_c for β-relaxation was increased by sucrose and decreased by isomaltose. Trehalose slightly decreased τ_c. The orders of τ_c and Ea for β-relaxation are as follows: sucrose > none > trehalose > isomaltose, although the standard errors in Ea make comparisons with pure lysozyme uncertain. These findings suggest that the mobility of the lysozyme carbonyl carbons is decreased by sucrose and increased by isomaltose. Because few data are available addressing the stability of freeze-dried lysozyme in the presence of sugars, the precise effect of sucrose on lysozyme stability is not known. However, the decrease in β-mobility brought about by sucrose may be related to the greater stabilizing effect of sucrose than trehalose, which was observed with some freeze-dried protein-sugar systems reported earlier (24,34).

The value of $T_{1\rho}$ minimum for the lysozyme carbonyl carbons shown in Table I varied with the sugars. The constant A in Eq. 1, which determines $T_{1\rho}$, is inversely proportional to the sixth power of the distance between the carbon and the proton that relaxes the carbon nuclei through dipole-dipole interaction (43). Thus, a small change in the distance between the carbon and proton nucleus results in a significant change in $T_{1\rho}$. The change in the estimated $T_{1\rho}$(min) caused by the addition of sugars suggests that the molecular structure of lysozyme is slightly changed by the sugars, such that the distance between the carbon and proton involved in nuclear relaxation is changed. The change in the value of $T_{1\rho}$ minimum caused by sucrose is smaller than that caused by trehalose and isomaltose, such that the change in the molecular structure of lysozyme caused by sucrose appears to be smaller than those caused by trehalose and isomaltose, which is curious in view of the fact that the apparent impact of sucrose on mobility (i.e., τ_c) is quite significant.

Table I Estimated Parameters of $T_{1\rho}$(min) and Ea for β- and γ-Relaxation, and Calculated τ_c Values at 25°C

Formulation	β -relaxation				γ-relaxation			
	τ_0 (s)	Ea (kJ/mol)	$T_{1\rho}$ (min) (ms)	τ_c (25°C) (ms)	τ_0 (s)	Ea (kJ/mol)	$T_{1\rho}$ (min) (ms)	τ_c (25°C) (μs)
lysozyme [a]	4×10^{-13} (2×10^{-12})	48 (14)	19 (4)	0.1	9×10^{-11} (2×10^{-10})	20 (4)	13 (3)	0.3
lysozyme-trehalose [b]	–	47 (1)	32 (7)	0.07	–	20 (0)	22 (2)	0.3
lysozyme-sucrose [c]	–	49 (1)	–	0.2	–	20 (0)	15 (2)	0.3
lysozyme-isomaltose [b]	–	43 (1)	28 (6)	0.02	–	20 (0)	20 (2)	0.3

() denotes standard error as provided by the non-linear regression

[a] Parameters of τ_0, Ea and $T_{1\rho}$(min) for each of the β- and γ-relaxation were evaluated by fit of the theoretical model (Eqs. 3 and 4) to the data.

[b] Parameters of Ea and $T_{1\rho}$(min) for each of the β- and γ-relaxation were estimated using the value of τ_0 obtained for lysozyme without sugars.

[c] The parameter Ea for β-relaxation was estimated using the values of τ_0 and $T_{1\rho}$(min) obtained for lysozyme without sugars, and parameters of Ea and $T_{1\rho}$(min) for γ-relaxation were estimated using the value of τ_0 obtained for lysozyme without sugars.

The value of apparent activation energy (i.e., temperature coefficient, Ea) determined for the β-relaxation of the lysozyme carbonyl carbons, shown in Table I, ranges between 43 to 50 kJ/mol, with the values for pure lysozyme and both the sucrose and trehalose systems being essentially the same but with the Ea for the isomaltose system being lower. By contrast, the Ea values for the γ-relaxation are all much smaller and essentially equal at around 20 kJ/mol. These Ea values are greater than those reported for fast dynamics of amorphous formulations determined by NMR relaxation measurements. For example, the apparent activation energy was determined to be 4.2 kJ/mol and 2.1 kJ/mol for the motion of the methine carbon in freeze-dried dextran and that of the protein carbonyl carbons in freeze-dried bovine serum γ-globulin, respectively, from NMR relaxation times (35). The dynamics of the PVP ring carbon and the sucrose methine carbon in freeze-dried PVP-sucrose mixtures, as determined by T_1 and $T_{1\rho}$, show apparent Ea values less than 10 kJ/mol. Moreover, the dynamics of the PVP ring carbon in freeze-dried PVP, determined by $T_{1\rho}$, exhibit a very small apparent Ea of 0.8 kJ/mol (36). These small apparent activation energies evaluated from the temperature dependence of NMR relaxation times, which are too small to be interpreted in terms of an activated state kinetic model, may be attributed to the invalid assumption that the atom of interest has only a single type of motion with a single τ_c value. When the atom has multiple types of motion with different τ_c values, the Ea value determined in a temperature range near $T_{1\rho}$ maximum according to this analysis has no sound theoretical foundation and may have no physical meaning as an activation energy. The analysis of NMR relaxation time according to a multiple-dynamic model, as described in this paper, is necessary to determine Ea for the individual type of motion. The value of Ea observed for freeze-dried lysozyme-sugar systems in this study is much smaller than the Ea for alpha relaxation for freeze-dried trehalose (145 kJ/mol) and freeze-dried sucrose (225 kJ/mol) as determined by isothermal microcalorimetry (28), calculated using $\beta=0.4$, but comparable to those for freeze-dried lactose by dielectric relaxation spectroscopy (72 kJ/mol and 52 kJ/mol for β- and γ-relaxation, respectively) (32).

The value of Ea determined for molecular motions in freeze-dried formulations is one of the basic clues for exploring the molecular motion most relevant to the instability of freeze-dried formulations. For example, if a certain motion shows an Ea value that is markedly different from the activation energy for degradation, it seems likely[1] that this motion may be excluded from the candidate motions responsible for the instability. The values of Ea determined for the β-relaxation of the lysozyme carbonyl carbons in this study are comparable to the values of activation energy for degradation observed for freeze-dried formulations as described below, suggesting correlations between β-relaxation and instability. Few data on activation energy have been reported for degradation in freeze-dried formulations, but Ea can be calculated from the Arrhenius plots of the apparent rate constants reported for degradation in freeze-dried formulations. For example, the Ea of the hydrolysis rate of cephalothin freeze-dried with dextran was calculated to be about 50 kJ/mol; Ea of 46 kJ/mol was calculated for acetyl transfer reaction between aspirin and sulfadiazine freeze-dried with poly(vinylpyrrolidone) (14). For degradation of freeze-dried proteins, 63 kJ/mol for aggregation of β-galactosidase freeze-dried with sugars (24), 50 kJ/mol for β-galactosidase freeze-dried with polyvinylalcohol (12), 67 kJ/mol for degradation of insulin freeze-dried with PVP (18).

[1] This statement is equivalent to stating that the motion represented by the relaxation process may have nothing directly to do with the motion required for degradation, if the "coupling coefficient" relating a relaxation time constant for a given microstate with degradation within that microstate, which has been discussed in a reference (6), is much less than unity.

Effect of Sub-T_g Heating on the Mobility of Lysozyme Carbonyl Carbons

Annealing of freeze-dried formulations at temperatures below and near the T_g is well known to increase α-relaxation time and to stabilize the formulations (41). For the freeze-dried lysozyme-trehalose and lysozyme-sucrose, the $T_{1\rho}$ value obtained immediately after the temperature was raised from −40°C to 62°C was close to the value determined at 62.3°C without heating or cooling (Fig. 3), as shown in Fig. 4. Thereafter, $T_{1\rho}$ decreased with time and became roughly constant within several hours. This finding suggests that the β- and γ-relaxations of lysozyme at the time point immediately after the temperature increase is different from those of lysozyme heated at 62°C for several hours.

As shown in Fig. 5, the $T_{1\rho}$ of the protein carbonyl carbons observed at temperatures below 0°C was not significantly affected by heating at 62°C for 8 h, but $T_{1\rho}$ above 0°C was greatly decreased by heating. The V-shaped temperature dependence of $T_{1\rho}$ for γ-relaxation was widened and moved toward a higher temperature range both for trehalose and sucrose. These findings suggest that the average τ_c for all carbonyl carbons in the lysozyme molecule is increased after heating and also that carbonyl carbons at different sites of the lysozyme molecule are affected by the heating treatment in varying degrees from each other, such that the range of τ_c for γ-relaxation of the lysozyme carbonyl carbons is widened. The effect of heating on the β-relaxation is not clear because of more limited $T_{1\rho}$ data. However, the finding that the $T_{1\rho}$ minimum for β-relaxation of the freeze-dried lysozyme-trehalose observed before heating is not observed after heating in the temperature range studied suggests that the $T_{1\rho}$ minimum for β-relaxation is shifted to a higher temperature by heating. Thus, both β- and γ-relaxations appear to be slowed by heating in a manner similar to the annealing effects on α-relaxations.

Mobility of Sugars Freeze-Dried with Lysozyme

The temperature dependence for the $T_{1\rho}$ of trehalose, sucrose and isomaltose carbons (Figs. 5 and 6) exhibits $T_{1\rho}$ minima in a similar temperature range as for the $T_{1\rho}$ of the lysozyme carbonyl carbons. This suggests that the sugar carbons have motions with similar τ_c values as the β- and γ-relaxation of the protein carbonyl carbons. Here, the values of $T_{1\rho}$ for the sucrose carbon are greater than those for the trehalose and isomaltose methine carbon. This is expected because the sucrose carbon (C-1) has no proton directly binding to the carbon, while trehalose and isomaltose methine carbons have a proton directly binding to the carbon. The rate of spin-lattice relaxation depends on the number of the protons that cause dipole-dipole interaction with the carbon, leading to spin-lattice relaxation, as well as the distance between the proton and the carbon (C-1). More protons and a shorter distance both lead to faster spin-lattice relaxation. The spin-lattice relaxation of sucrose carbon (C-1) is slower than that of trehalose and isomaltose, because the proton involved in the dipole-dipole interaction with the carbon (C-1) in the sucrose system is at a greater distance from the carbon compared to the trehalose and isomaltose systems.

The temperature dependence for the $T_{1\rho}$ of sugar carbons was not significantly changed by the addition of lysozyme. This finding means that the motions of sugar carbons with similar τ_c values as the β- and γ-relaxation of the protein carbonyl carbons are not affected by interaction with lysozyme. This finding is in contrast to the observation that the β- and γ-relaxations of the lysozyme carbonyl carbons are affected by interaction with the sugars (Table I). This difference may be explained by assuming that the sugar induces conformational changes in the protein, such that the mobility of the protein carbonyl carbons is significantly changed but mobility of the sugar carbon is changed by interaction with the protein only for the carbons involved in the interaction. Mobility of the carbons that are not involved in the interaction also contributes to the determined $T_{1\rho}$ value, such that the measured $T_{1\rho}$ for the sugar is not sensitive to the interaction with protein.

The $T_{1\rho}$ of the methyl carbon of ^{13}C-methylated isomaltose decreases rapidly as temperature increases near and above T_g (Fig. 7). This finding suggests that the motion of the methyl carbon, which is speculated to be much faster than the carbon (C-1), is coupled with structural relaxation since structural relaxation shows strong temperature dependence near T_g. This observation is in contrast to the general concept that the fast motion of side chains is generally independent of structural relaxation.

CONCLUSION

The temperature dependence for the $T_{1\rho}$ of the lysozyme carbonyl carbons in freeze-dried lysozyme with and without sugars (trehalose, sucrose and isomaltose) was describable with a model that assumes that the carbon has two different types of molecular motion with different τ_c values and that each τ_c shows an Arrhenius type of temperature dependence. A single relaxation mode is not consistent with the data, meaning that interpretation of relaxation time data is complex and may demand data over an extended temperature range. If $T_{1\rho}$ is determined in a temperature range near $T_{1\rho}$ maximum, simply observing that an increase in temperature reduces $T_{1\rho}$ does not necessarily mean that the

$T_{1\rho}$ measured is directly proportional to the correlation time, τ_c, nor is the temperature coefficient of $T_{1\rho}$ necessarily a good measure of the activation energy of a single process. Further, trends in $T_{1\rho}$ with formulation determined in this temperature range may not necessarily be predictive of trends in molecular mobility.

Lysozyme carbonyl carbons in the absence of sugars revealed two types of motion with much smaller values of τ_c and Ea than structural relaxation: a motion with a τ_c of 1×10^{-4} s at 25°C and an Ea of 48 kJ/mol (β-relaxation), and another faster motion with a τ_c of 3×10^{-7} s at 25°C and an Ea of 20 kJ/mol (γ-relaxation). Addition of sugars does impact the mobility of lysozyme, as evidenced by the impact of sugars on the values of τ_c and Ea. The τ_c and Ea for β-relaxation were increased by the addition of sucrose and decreased by the addition of trehalose and isomaltose. The orders of τ_c and Ea are as follows: sucrose > none > trehalose > isomaltose, suggesting that the β-mobility of the lysozyme carbonyl carbons is significantly decreased by sucrose but increased by isomaltose.

REFERENCES

1. Yoshioka S, Aso Y. Correlation between molecular mobility and chemical stability during storage of amorphous pharmaceuticals. J Pharm Sci. 2007;96:960–81.
2. Craig DQM, Royall PG, Kett VL, Hopton ML. The relevance of the amorphous state to pharmaceutical dosage forms: glassy drugs and freeze dried systems. Int J Pharm. 1999;179:179–207.
3. Wang W. Lyophilization and development of solid protein pharmaceuticals. Int J Pharm. 2000;203:1–60.
4. Parker R, Gunning YM, Lalloué B, Noel TR, Ring SG. Glassy state dynamics, its significance for biostabilization and role of carbohydrates. In: Levine H, editor. Amorphous food and pharmaceutical systems. Cambridge: The Royal Society of Chemistry; 2002. p. 73–87.
5. Pikal MJ. Chemistry in solid amorphous matrices: implication for biostabilization. In: Levine H, editor. Amorphous food and pharmaceutical systems. Cambridge: The Royal Society of Chemistry; 2002. p. 257–72.
6. Pikal MJ. Mechanisms of protein stabilization during freeze-drying and storage: the relative importance of thermodynamic stabilization and glassy state relaxation dynamics. In: Rey L, May JC, editors. Freeze-drying/lyophilization of pharmaceutical and biological products. 2nd ed. New York: Marcel Dekker Inc; 2004. p. 63–107.
7. Shamblin SL. The role of water in physical transformations in freeze-dried products. In: Costantino HR, Pikal MJ, editors. Lyophilization of biopharmaceuticals. Arlington: AAPS; 2004. p. 229–70.
8. Lechuga-Ballesteros D, Miller DP, Dudddu SP. Thermal analysis of lyophilized pharmaceutical peptide and protein formulations. In: Costantino HR, Pikal MJ, editors. Lyophilization of biopharmaceuticals. Arlington: AAPS; 2004. p. 271–335.
9. Stots CE, Winslow SL, Houchin ML, D'Souza AJM, Ji J, Topp EM. Degradation pathways for lyophilized peptides and proteins. In: Costantino HR, Pikal MJ, editors. Lyophilization of biopharmaceuticals. Arlington: AAPS; 2004. p. 443–79.
10. Sun WQ, Davidson P, Chan HSO. Protein stability in the amorphous carbohydrate matrix: relevance to anhydrobiosis. Biochim Biophys Acta. 1998;1425:245–54.
11. Yoshioka S, Aso Y, Nakai Y, Kojima S. Effect of high molecular mobility of poly(vinyl alcohol) on protein stability of lyophilized γ-globulin formulations. J Pharm Sci. 1998;87:147–51.
12. Yoshioka S, Tajima S, Aso Y, Kojima S. Inactivation and aggregation of β-galactosidase in lyophilized formulation described by Kohlrausch-Williams-Watts stretched exponential function. Pharm Res. 2003;20:1655–60.
13. Lai MC, Hageman MJ, Schowen RL, Borchardt RT, Laird BB, Topp EM. Chemical stability of peptide in polymers. 2. Discriminating between solvent and plasticizing effects of water on peptide deamidation in poly(vinylpyrrolidone). J Pharm Sci. 1999;88:1081–9.
14. Yoshioka S, Aso Y, Kojima S. Temperature- and glass transition temperature-dependence of bimolecular reaction rates in lyophilized formulations described by the Adam-Gibbs-Vogel equation. J Pharm Sci. 2004;93:1062–9.
15. Guo Y, Byrn SR, Zografi G. Physical characteristics and chemical degradation of amorphous quinapril hydrochloride. J Pharm Sci. 2000;89:128–43.
16. Yoshioka S, Aso Y. A quantitative assessment of the significance of molecular mobility as a determinant for the stability of lyophilized insulin formulations. Pharm Res. 2005;22:1358–64.
17. Yoshioka S, Miyazaki T, Aso Y. Degradation rate of lyophilized insulin, exhibiting an apparent arrhenius behavior around glass transition temperature regardless of significant contribution of molecular mobility. J Pharm Sci. 2006;95:2684.
18. Yoshioka S, Aso Y, Miyazaki T. Negligible contribution of molecular mobility to the degradation rate of insulin lyophilized with poly(vinylpyrrolidone). J Pharm Sci. 2006;95:939–43.
19. Strickley RG, Anderson BD. Solid-state stability of human insulin II. Effect of water on reactive intermediate partitioning in lyophiles from pH 2–5 solutions: stabilization against covalent dimer formation. J Pharm Sci. 1997;86:645–53.
20. Yoshioka S, Miyazaki T, Aso Y. β-relaxation of insulin molecule in lyophilized formulations containing trehalose or dextran as a determinant of chemical reactivity. Pharm Res. 2006;23:961–6.
21. Chang L, Shepherd D, Sun J, Ouellete D, Grant KL, Tang X, *et al.* Mechanism of protein stabilization by sugar during freeze-drying and storage: native structure preservation, specific interaction, and/or immobilization in a glassy matrix? J Pharm Sci. 2005;94:1427–44.
22. Cicerone MS, Soles C. Fast dynamics and stabilization of proteins: binary glasses of trehalose and glycerol. Biophys J. 2004;86:3836–45.
23. Cicerone MT, Soles CL, Chowdhuri Z, Pikal MJ, Chang LL. Fast dynamics as a diagnostic for excipients in preservation of dried proteins. Am Pharm Rev. 2005;8:24–7.
24. Yoshioka S, Miyazaki T, Aso Y, Kawanishi T. Significance of local mobility in aggregation of β-galactosidase lyophilized with trehalose, sucrose or stachyose. Pharm Res. 2007;24:1660–7.
25. Matsuo M, Bin Y, Xu C, Ma L, Nakaoki T, Suzuki T. Relaxation mechanism in several kinds of polyethylene estimated by dynamic mechanical measurements, positron annihilation, X-ray and ^{13}C solid-state NMR. Polymer. 2003;44:4325–40.
26. Aso Y, Yoshioka S. Effect of freezing rate on physical stability of lyophilized cationic liposomes. Chem Pharm Bull. 2005;53:301–4.
27. Andronis V, Zografi G. Molecular mobility of supercooled amorphous indomethacin, determined by dynamic mechanical analysis. Pharm Res. 1991;14:410–4.
28. Liu J, Rigsbee DR, Stotz C, Pikal MJ. Dynamics of pharmaceutical amorphous solids: the study of enthalpy relaxation by isothermal microcalorimetry. J Pharm Sci. 2002;91:1853–62.

29. Shamblin SL, Tang X, Chang L, Hancock BC, Pikal MJ. Characterization of the time scales of molecular motion in pharmaceutically important glasses. J Phys Chem B. 1999;103:4113–21.
30. Kumagai H, Sugiyama T, Iwamoto S. Effect of water content on dielectric relaxation of gelatin in a glassy state. J Agric Food Chem. 2000;48:2260–5.
31. Yoshioka S, Aso Y. Glass transition- related changes in molecular mobility below glass transition temperature of freeze-dried formulations, as measured by dielectric spectroscopy and solid state nuclear magnetic resonance. J Pharm Sci. 2005;94:275–87.
32. Ermolina I, Polygalov E, Bland C, Smith G. Dielectric spectroscopy of low-loss sugar lyophiles: II. Relaxation mechanisms in freeze-dried lactose and lactose monohydrate. J Non-Crystalline Solids. 2007;353:4485–91.
33. Correia NT, Ramos JJM, Descamps M, Collins G. Molecular mobility and fragility inindomethacin: a thermally stimulated depolarization current study. Pharm Res. 2001;18:1767–74.
34. Pikal MJ, Rigsbee D, Roy ML, Galreath D, Kovach KJ, Wang B, *et al.* Solid state chemistry of proteins: II. the correlation of storage stability of freeze-dried human growth hormone (hGH) with structure and dynamics in the glassy solid. J Pharm Sci. 2008;97:5106–21.
35. Yoshioka S, Aso Y, Kojima S, Sakurai S, Fujiwara T, Akutsu H. Molecular mobility of protein in lyophilized formulations linked to the molecular mobility of polymer excipients, as determined by high resolution ^{13}C solid-state NMR. Pharm Res. 1999;16:1621–5.
36. Aso Y, Yoshioka S, Zhang J, Zografi G. Effect of water on the molecularmobility of sucrose and poly(vinylpyrrolidone) in a colyophilized formulation as measured by ^{13}C-NMR relaxation time. Chem Pharm Bull. 2002;50:822–6.
37. Latosinska JN, Latosinska M, Utrecht R, Mielcarek S, Pietrzak J. Molecular dynamics of solid benzothiadiazine derivatives (Thiazides). J Molecular Structure. 2004;694:211–7.
38. Nichaus Jr WG, Ryhage R. Determination of double bond positions in polyunsaturated fatty acids by combination gas chromatography-mass spectrometry. Anal Chem. 1968;40:1840–7.
39. Bielecki A, Burum DP. Temperature dependence of ^{207}Pb MAS spectra of solid lead nitrate. An accurate, sensitive thermometer for variable-temperature MAS. K Magnetic Res Ser A. 1995;116:215–20.
40. Pfeffer PE, Odier L, Dudley RL. Assignment of ^{13}C CPMAS NMR spectra of crystalline methyl β-D-glucopyranoside and sucrose using deuterium labeling and interrupted proton decoupling. J Carbohydrate Chem. 1990;9:619–29.
41. Wang B, Cicerone MT, Aso Y, Pikal MJ. The impact of thermal treatment on the stability of freeze-dried amorphous pharmaceuticals: II. Aggregation in an IgG1 fusion protein. J Pharm Sci. 2010;99:683–700.
42. Iijima T, Mizuno M, Suhara M, Endo K. Molecular and electron-spin dynamics in $[M(H_2O)_6][AB_6]$ as studied by solid state NMR. Bunseki Kagaku. 2003;52:157–63.
43. Horii F. NMR relaxation and dynamics. In: Ando I, Asakura T, editors. Solid state NMR of polymers. Amsterdam: Elsevier; 1998. p. 51–81.

RESEARCH ARTICLE

Feasibility of Atomic Force Microscopy for Determining Crystal Growth Rates of Nifedipine at the Surface of Amorphous Solids with and Without Polymers

TAMAKI MIYAZAKI, YUKIO ASO, TORU KAWANISHI

Division of Drugs, National Institute of Health Sciences, Setagaya-ku, Tokyo 158-8501, Japan

Received 21 February 2011; revised 31 March 2011; accepted 18 April 2011

Published online in Wiley Online Library (wileyonlinelibrary.com). DOI 10.1002/jps.22603

ABSTRACT: Amorphous nifedipine (NFD), which has a smooth surface immediately after preparation, was shown to have structures resembling clusters of curling and branching fibers approximately 1 μm wide by atomic force microscopy (AFM) after storage at 25°C. The size of the cluster-like structures increased with storage over time, implying crystal growth. The average elongation rate of the fibers determined by AFM at ambient room temperature was 1.1×10^{-9} m/s, and this agreed well with the crystal growth rate of 1.6×10^{-9} m/s determined by polarized light microscopy. The crystal growth rate of NFD in solid dispersions with 5% polyethylene glycol (PEG) was found to be 5.0×10^{-8} m/s by AFM. Although this value was approximately the same as that obtained by polarized light microscopy, three-dimensional information obtained by AFM for the crystallization of NFD in a solid dispersion with PEG revealed that the changes in topography were not a consequence of surface crystal growth, but rather attributable to the growth of crystals formed in the amorphous bulk. For solid dispersions with α,β-poly(N-5-hydroxypentyl)-L-aspartamide, acceleration of NFD crystallization by tapping with an AFM probe was observed. The present study has demonstrated the feasibility and application of AFM for interpretation of surface crystallization data. © 2011 Wiley-Liss, Inc. and the American Pharmacists Association J Pharm Sci

Keywords: amorphous; crystallization; excipients; physical stability; solid dispersion; microscopy

INTRODUCTION

Amorphous drugs are generally more soluble and dissolve faster than their crystalline counterparts.[1–3] Therefore, amorphization of poorly water-soluble drugs is a useful method for enhancing their dissolution rate and consequently improving their bioavailability. However, the amorphous form is thermodynamically unstable and tends to revert to its crystalline form, resulting in loss of the solubility advantage. Recently, surface-enhanced crystallization of indomethacin[4] and nifedipine (NFD)[5] has been reported. The crystal growth rates of amorphous indomethacin and NFD at the free surface were orders of magnitude faster than those in bulk at temperatures below their glass transition temperature (T_g). Microscopic observation of partially crystallized indomethacin and NFD samples has revealed that crystallized drugs are localized at the surface of the samples.[5] Once the surface is covered with a crystal layer, the solubility advantage is lost even if the most interior part of the solid remains amorphous.

Atomic force microscopy (AFM), which can capture surface topography images of solid samples with a resolution of the micrometer order or less, may be a useful tool for investigating the surface crystallization of pharmaceuticals. The crystallization of cholesterol under conditions simulating the gallbladder environment has been studied by AFM.[6] Cholesterol crystals of submicrometer size have been observed on the surface of mica and mucin-coated mica, but no such crystals have been found on the surface of silanized mica, suggesting that a network of hydrogen bonds on the surface provides favorable conditions for the nucleation and growth of cholesterol crystals. Molecular rearrangements at the surface have been observed for caffeine/carboxylic acid cocrystals by AFM.[7] The depth and width of trenches aligned

Correspondence to: Tamaki Miyazaki (Telephone: +81-3-3700-1141; Fax: +81-3-3707-6950; E-mail: miyazaki@nihs.go.jp)

Journal of Pharmaceutical Sciences

along the needle-shaped crystal axis have been shown to increase during storage for 2–7 days under dry and humid conditions, and regular triangular or rectangular features have been observed, indicating surface recrystallization of caffeine cocrystals. Changes in the surface topology of spray-dried lactose particles have also been observed by AFM.[8] Linear striated features due to crystallization appeared and gradually propagated across the surface of the particles stored at 58% relative humidity. The crystallized surface had an irregular topology with a well-ordered and definable structure over relatively small areas but not over wide areas, suggesting that secondary nucleation and growth had occurred. Furthermore, the surface crystallization rate of spray-dried amorphous lactose has been reported.[9,10] Images of rectangular shapes on the surface of the lactose particles have been sequentially captured as a function of time by AFM, and the growth rate has been estimated from the time profiles of width and length of the rectangular shapes.

The aim of this study was to investigate the feasibility of AFM for determining crystal growth rates at the surface of amorphous NFD in the presence and absence of polymer excipients by capturing sequential images in specific areas of the samples. The polymer excipients used were polyethylene glycol (PEG) and α,β-poly(N-5-hydroxypentyl)-L-aspartamide (PHPA). PEG is one of the typical polymers used for preparation of solid dispersions to improve drug dissolution.[11–13] PHPA has been selected as a model of a partially immiscible polymer with NFD[14] because the miscibility of an amorphous drug with polymer excipients is one of the factors that determine the physical stability of amorphous solid dispersions.[15] Here, we compared the growth rates estimated from AFM measurements with the values estimated from polarized light microscopy measurements. Spatial information on the crystallization of NFD alone and that in these solid dispersions obtained by AFM is described.

EXPERIMENTAL

Materials and Sample Preparation

Nifedipine was obtained from Sigma–Aldrich Company (St. Louis, MO). PEG with an average molecular weight of 300 was purchased from Wako Pure Chemical Industries Ltd. (Osaka, Japan). PHPA was synthesized via polycondensation of L-aspartic acid and 1-aminopentane using a method similar to that reported previously.[16]

The sample of amorphous NFD was prepared on a glass plate as follows: Crystalline NFD (approximately 20 mg) was put on a glass plate (thickness 0.12–0.17 mm, diameter 18 mm), and the plate was placed in a differential scanning calorimeter (DSC2920; TA Instruments, New Castle, DE) at 190°C for approximately 2 min under dry nitrogen flow (30 mL/min). Then, the glass plate was removed from the differential scanning calorimeter and cooled to room temperature on a stainless steel block for several seconds. The samples were stored in a desiccator over phosphorous pentoxide to avoid moisture, and were kept at 25°C before AFM measurements. Amorphous NFD samples containing PEG or PHPA were prepared as described above using approximately 20 mg of NFD–polymer mixtures, which were obtained by solvent evaporation of NFD–PEG methanol solution and NFD–PHPA ethanol solution.

Amorphous NFD containing PEG was also prepared in a glass Petri dish (inner diameter 23 mm, depth 7 mm) to visually examine positions of NFD crystallization in the NFD–PEG solid dispersion. Approximately 2 g of NFD–PEG (5%) mixture in the Petri dish was kept at 197°C for 5 min in an oven, and then quenched on a stainless steel block that had been precooled with ice.

AFM Measurements

Atomic force microscopy (Dimension 3100; Veeco Instruments, Plainview, NY) measurements were performed in tapping mode, analogous to noncontact mode and alternating current mode, under ambient temperature (26±1°C) and relative humidity (<50%). The operation software used was Nanoscope 5.30r1 (Veeco Instruments). Silicon probes with a nominal spring constant of 42 N/m and a nominal length of 125 μm were used. AFM images were collected at a scan speed of 50–150 μm/s for a square region of 50–100 μm with 256–512 collecting points per line. The topography images were collected by scanning the probe across the surface of the sample in a raster pattern, line by line, from one side of the square area toward the opposing side. Because the scan direction changed alternately from downward and upward during sequential data collection, only the images collected in the downward scan direction were used to determine the crystal growth rate. To investigate the potential effects of physical stimulation from the AFM probe on the crystal growth rate of NFD, AFM images were collected at various time intervals (1.3–17 min/image) by varying the scan range, scan speed, and collecting points per line.

Measurements of Crystal Growth Rate by Polarized Light Microscopy

Crystal growth rates of NFD in amorphous NFD alone and NFD–polymer solid dispersions were determined using a polarized light microscope (ECLIPSE E600 POL; Nikon Corporation, Tokyo, Japan) with a ×10 objective lens (depth of field 8.46 μm). The microscope was equipped with a heating/cooling

 DOI 10.1002/jps

stage (THMS600; Linkam Scientific Instruments, Tadworth, Surrey, UK) to control the temperature of the sample. The sample of amorphous NFD, prepared as described above, was placed in the chamber of the heating/cooling stage, which had been preheated to 25°C. Then, the chamber was purged with dry nitrogen gas for 5–10 min to remove moisture, and hermetically closed. The focus of the microscope was adjusted to the free surface of the amorphous sample, and the crystal growth was observed. Microscopy images were recorded at constant time intervals by a digital camera (DXM1200F; Nikon Corporation) attached to the microscope, and were analyzed using Lumina Vision software (Mitani Company, Fukui, Japan). The crystal growth rates were estimated from the increase in size of the crystals with storage time.

Differential Scanning Calorimetry Measurements

Glass transition temperature values of the amorphous NFD and NFD–polymer solid dispersions were determined by differential scanning calorimetry (DSC) measurement. Indium was used to calibrate the cell constant and the temperature of the instrument. The DSC cell was purged constantly by dry nitrogen gas flow at 30 mL/min. Crystalline NFD or NFD–polymer mixed powder (approximately 5 mg) in a hermetic aluminum pan was heated to 190°C at a heating rate of 20°C/min, kept at that temperature for 90 s, and then cooled to −80°C at a cooling rate of 40°C/min by pouring liquid nitrogen into a cooling jacket surrounding the DSC cell. The T_g was obtained on the second heating run at a rate of 20°C/min.

The melting point of recrystallized NFD was measured by DSC. After AFM observation, the sample was stored in a desiccator over phosphorous pentoxide at 25°C to complete the recrystallization. Completion of the recrystallization took approximately 3 months for pure NFD, 1 month for NFD–PEG solid dispersions, and a $\frac{1}{2}$ year for NFD–PHPA solid dispersions. The recrystallized sample (5–10 mg) was scratched off from the glass plate into a hermetic aluminum pan, and the melting point of the sample was measured at a heating rate of 20°C/min.

RESULTS AND DISCUSSION

Amorphous NFD Without Polymer

Figure 1 shows typical AFM images of amorphous NFD. Amorphous NFD exhibited a smooth surface immediately after preparation as shown in Figure 1a. The root-mean-square value of the surface roughness was less than 0.5 nm for freshly prepared amorphous samples. After storage at 25°C, structures resembling clusters of curling and branching fibers with a width of approximately 1 μm appeared on the surface as shown in Figure 1b. The size of these structures increased with storage time, suggesting that they were NFD crystals that had formed during storage. The height of the crystals was approximately 1 μm, and hardly this changed even when the scanning area for AFM was covered by NFD crystals. This suggested that NFD crystals preferentially grew along the surface than toward the inner part of the sample. This speculation is supported by the fact that the inner part of the NFD sample after AFM measurements was transparent, indicating that the interior of the samples remained amorphous even after the surface had crystallized. Faster crystal growth of NFD at the surface of amorphous solids has been reported by Zhu et al.[5] They found that the crystal growth of NFD occurred preferentially at the free surface of the amorphous sample when it was exposed to air by removing one glass plate from a sample that had been prepared between two glass plates. The crystal shape reported by Zhu et al.[5] was similar to that shown in Figure 1b.

The crystal form of NFD observed by AFM was determined from the melting point of the recrystallized samples. Figure 2 shows DSC thermograms of crystalline NFD and completely recrystallized NFD, which had been stored as amorphous NFD at 25°C for approximately 3 months after AFM measurements. The recrystallized NFD showed an endothermic peak at approximately 171°C (Fig. 2b), suggesting that a stable form of NFD crystal (Fig. 2a) is formed during storage at 25°C.

Serial AFM images of partially recrystallized amorphous NFD were captured continuously in the same area to determine the crystal growth rate of NFD at

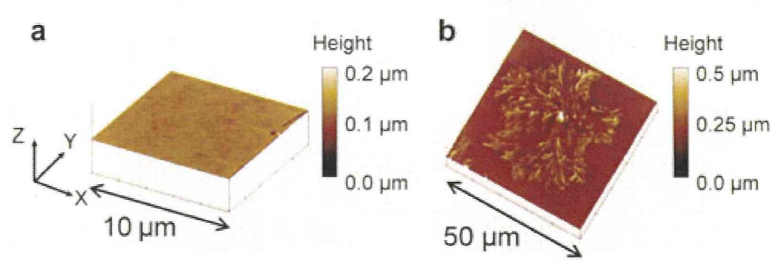

Figure 1. Representative atomic force microscopy images of amorphous nifedipine (a) immediately after preparation and (b) after storage at 25°C.

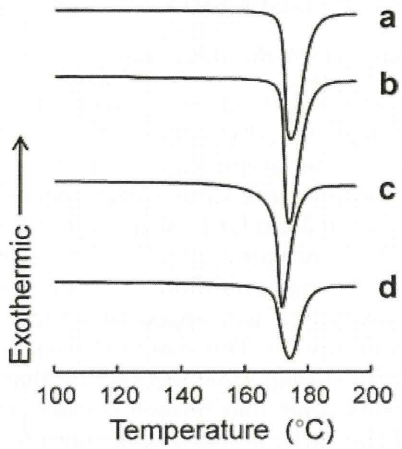

Figure 2. Differential scanning calorimeter thermograms for (a) nifedipine (NFD) in stable form, NFD recrystallized at 25°C from amorphous (b) NFD without polymer, (c) NFD–polyethylene glycol (5%) solid dispersion, and (d) NFD–α,β-poly(N-5-hydroxypentyl)-L-aspartamide (30%) solid dispersion.

the surface. Figure 3 shows typical images representing crystal growth of NFD at the surface. The time required to capture one image was approximately 17 min for this series of measurements. Using image analysis software, the crystal growth rate was determined from the coordinates (x_A, y_A) and (x_B, y_B), which are the end points of one crystal indicated by A in the image after 68 min and B in the image after 102 min, respectively. The growth rate was calculated by dividing the distance between (x_A, y_A) and (x_B, y_B) by the time interval, 34 min. In order to confirm that the physical stimulation from the AFM probe did not affect the crystal growth rate of NFD, AFM images were collected at various time intervals by varying the experimental conditions (scan range, scan speed, and collecting points per line). If the physical stimulus of tapping affected the crystal growth, the estimated growth rates have differed depending on the interval employed for image collection. Growth rates estimated under various experimental conditions are shown in Table 1. Because differences in the estimated growth rates lay within experimental error range regardless of the interval used for image collection, any influence of tapping by the AFM probe on the crystal growth rate was considered to be negligible. The NFD crystal growth rate was also estimated by polarized light microscopy using some pairs of micrographs recorded when the microscope was focused on the surface of the amorphous solid (Table 1). The crystal growth rates of NFD determined from the data obtained by AFM and polarized light microscopy agreed well, and the growth rates determined in the present study were similar to those reported by Zhu et al.[5] for the crystal growth rate at the free surface of amorphous NFD solids.

NFD Solid Dispersions with PEG

The surface of NFD solid dispersions containing PEG was smooth immediately after preparation (images not shown). Figure 4 shows representative AFM images after storage at 25°C for approximately 1 day. NFD–PEG (5%) solid dispersions exhibited dimples at the surface, as shown in Figure 4a. Dimples with a depth of more than 5.7 μm (the operational limit of the AFM probe) were sometimes observed. After longer storage, spiky structures were observed in the dimples, as shown in Figure 4b, and the area with an apparently rough surface increased with time. Crystals were detected by polarized light microscopy in the positions where the dimples, with and without spiky structures, had been observed by AFM. This implies that the formation of dimples and spiky structures is associated with NFD crystallization during storage. Figure 5 shows a partially crystallized NFD–PEG (5%) solid dispersion prepared in a small glass Petri dish. After storage at 25°C for approximately 15 h, some crystals grew at the surface, as circled by dotted lines (Fig. 5a), although most of them were observed randomly in the bulk (Figs. 5a and 5b). These results indicated that NFD crystallization was not always initiated at the surface of NFD–PEG solid dispersions. The dimples at the surface observed by AFM may have been formed by volume reduction upon crystallization of amorphous NFD initiated in the bulk, but not so far from the sample surface. Therefore, it may take some time for the crystals with spiky structures to become apparent at the sample surface, as shown in Figure 4b. These results suggest that AFM measurements discriminate the position where crystallization has initiated (at the surface or in the bulk), and the

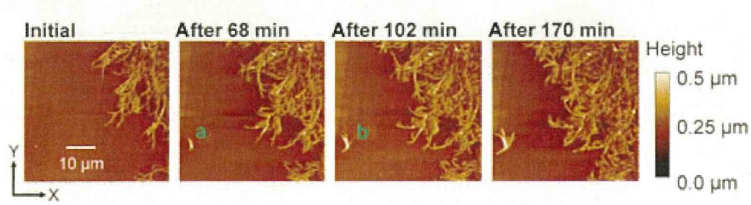

Figure 3. Serial atomic force microscopy images representing crystal growth at the surface of amorphous nifedipine without polymer at ambient temperature (26 ± 1°C).

 DOI 10.1002/jps

Table 1. T_g Values Determined by DSC, and NFD Crystal Growth Rates Obtained by AFM and Polarized Light Microscopy at Around 25°C

		AFM Experimental Conditions				Crystal Growth Rate (m/s)	
	T_g (°C)	Scan Range (μm)	Scan Speed (μm/s)	Collected Points Per Line	Collection Interval[a] (min)	AFM	Polarized Light Microscopy
NFD	46.2 ± 0.5[b]	100	75	256	5.3	(1.2 ± 0.3) × 10^{-9}[c]	(1.6 ± 0.4) × 10^{-9}[d]
		100	50	256	8.6	(1.1 ± 0.3) × 10^{-9}[c]	
		50	50	512	8.6	(1.0 ± 0.2) × 10^{-9}[c]	
		100	50	512	17	(1.3 ± 0.4) × 10^{-9}[c]	
NFD–PEG (5%)	33.5 ± 0.6[b]	100	150	256	2.6	5.1 × 10^{-8}	(7.2 ± 1.7) × 10^{-8}[e]
		80	150	256	2.2	6.3 × 10^{-8}	
		50	150	256	1.3	4.9 × 10^{-8}	
		100	100	256	4.3	4.5 × 10^{-8}	

[a]Time required to collect one image.
[b]Average with standard deviation ($n = 5$).
[c]Average with standard deviation ($n > 9$ points for each five samples).
[d]Average with standard deviation ($n > 5$ points for each five samples).
[e]Average with standard deviation ($n = 6$).
AFM, atomic force microscopy; NFD, nifedipine; PEG, polyethylene glycol.

direction of crystal growth (along the surface or into the bulk): characteristics that are difficult to determine by polarized light microscopy. It should be noted that even though AFM images suggest that crystals grow at the surface of samples, crystallization is not always initiated at the surface.

Although the crystal growth rate of NFD in a solid dispersion with PEG determined by AFM is not the surface growth rate, as described above, the apparent rate was estimated and compared with that obtained by polarized light microscopy. From serial AFM images exemplified by Figure 4b, the crystal growth rate of NFD in solid dispersions containing 5% PEG was determined. Because of possible changes in the NFD crystallization rate by the physical stimulus of tapping, the increase in diameter of the recrystallized domains was measured at various time intervals by varying the experimental scan range (50–100 μm) and scan speed (100–150 μm/s). Figure 6 shows the time profiles of the diameter of the recrystallized domains measured under various experimental conditions: hollow triangles and hollow squares represent the results of measurements using the shortest and the longest time intervals, respectively. The variation in slope appeared to lie within the range of experimental error, and no clear dependence of the growth rate on the time interval for collection was evident. From these results, it is considered that the influence of tapping by the AFM probe on the crystal growth rate is negligible in NFD–PEG solid dispersions. Each growth rate calculated from the slope of the plots shown in Figure 6 is listed in Table 1. The value was of the same order as that obtained by polarized light microscopy at 25°C (Table 1). The crystal growth rate of NFD in the NFD–PEG (5%) solid dispersions was approximately 50 times higher than that in amorphous NFD alone. The T_g value of the NFD–PEG (5%) solid dispersion was approximately 13° lower than that of NFD alone (Table 1), indicating that the matrix mobility of NFD–PEG is higher than that of NFD alone.

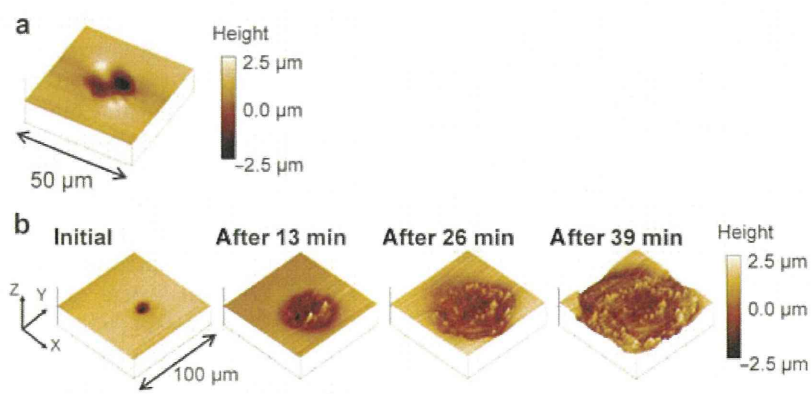

Figure 4. Atomic force microscopy images of nifedipine (NFD)–polyethylene glycol (5%) solid dispersion. (a) Partially recrystallized solid dispersion after storage at 25°C and (b) serial images representing NFD crystal growth at ambient temperature, 26 ± 1°C.

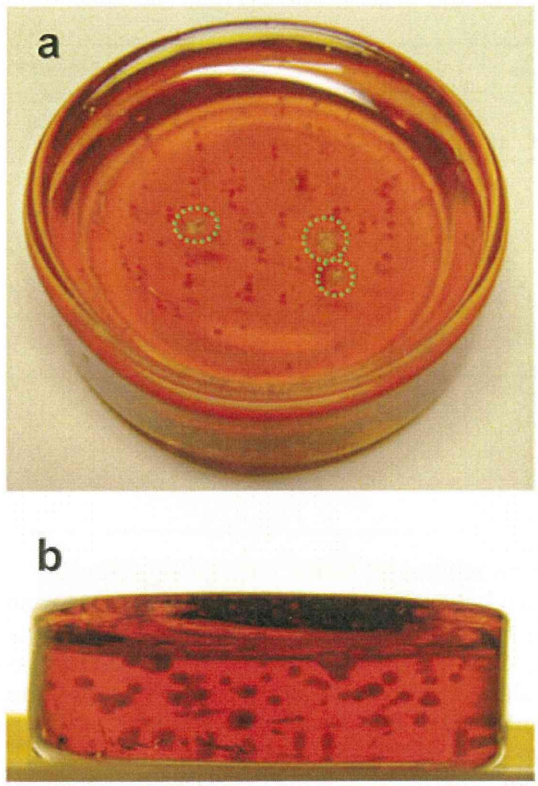

Figure 5. Partially crystallized nifedipine (NFD)–polyethylene glycol (5%) solid dispersion prepared in a small glass Petri dish (inner diameter 23 mm). The sample was stored at 25 C for approximately 15 h. Dotted green circles in the photograph (a) indicate sites of crystallization at the surface. Other dark granular shapes are NFD crystals formed in the amorphous bulk. (a) Photograph taken from top and (b) photograph taken from the side.

The increased molecular mobility of the amorphous matrix may be one of the reasons for the higher crystal growth rate in NFD–PEG solid dispersions. Another possible reason for the higher crystal growth rate may be due to the difference in the crystalline form formed in pure NFD and NFD–PEG solid dispersions during AFM measurements. Although the melting point of the recrystallized NFD in the solid dispersions containing PEG [169°C (Fig. 2c)] suggests that a stable form of NFD crystal is formed during the storage for 1 month, this result may not exclude the possibility that crystals other than stable form have been formed in the solid dispersions during AFM measurements.

NFD Solid Dispersions with PHPA

Figure 7a shows a typical AFM image of partially recrystallized NFD–PHPA solid dispersions stored at 25°C for a few weeks. The diameter and height of the cone-shaped structures increased with storage time.

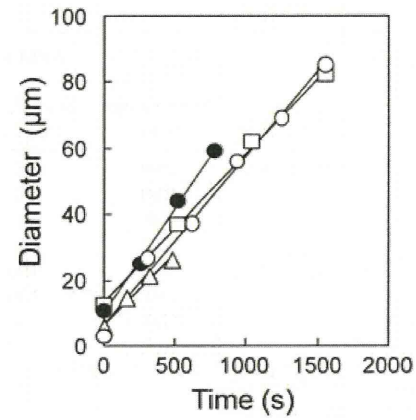

Figure 6. Increase in diameter of crystallized domains at the surface of nifedipine–polyethylene glycol (5%) solid dispersions at ambient temperature, 26 ± 1°C. The time when the first scan had been completed was defined as "time = 0" for each sequential measurement. The measurement conditions for each symbol are as follows (scan range and scan speed): ○ (100 μm, 150 μm/s), ● (80 μm, 150 μm/s), △ (50 μm, 150 μm/s), and □ (100 μm, 100 μm/s).

The melting point of the recrystallized NFD–PHPA (30%) samples stored at 25°C for approximately 6 months (169°C as shown in Fig. 2d) suggests that the crystal with a cone-shaped structure is the stable form of NFD.

Only the cone-shaped structures were observed in the first scan (Fig. 7a), but string-like structures were also observed in the image of the second scan (Fig. 7b). The area covered by the string-like structures increased gradually with each scan, as shown in Figure 7c, which is the image collected after continuous scanning for 34 min. Visual inspection of the area where AFM images were collected revealed loss of transparency in the area, suggesting crystallization of NFD. During the measurements, the size of the originally existing cone-shaped structures did not change (images not shown). Figure 7d shows an image of a different site in the same sample, wherein the AFM probe had not made contact, obtained after scanning the image shown in Figure 7c. No string-like structures were evident. These results suggest that physical stimulation by tapping with the AFM probe caused acceleration of new NFD crystal formation and growth at the surface of solid dispersions containing 30% PHPA. This acceleration effect was also observed for solid dispersions containing up to 70% PHPA. The reason why tapping by the AFM probe only accelerates the formation and growth of string-like crystals is still unclear. NFD is partially immiscible with PHPA. The presence of at least two different phases in the solid dispersion was indicated by the biexponential decay patterns of ^{1}H NMR spin-lattice relaxation.[14]

DOI 10.1002/jps

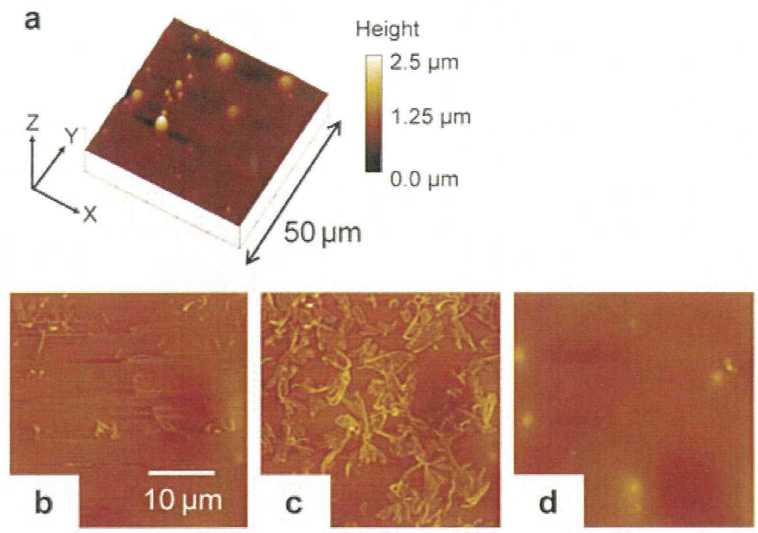

Figure 7. Atomic force microscopy images of nifedipine–α,β-poly(N-5-hydroxypentyl)-L-aspartamide (30%) solid dispersion. (a) The first scan of the partially crystallized sample stored at 25 C for over 1 month, (b) the second scan, (c) after continuous scanning for 34 min, (d) a different site in the same sample after measurement (c). The area for images (b) and (c) corresponds to approximately one-fourth of the bottom-right corner of the image (a).

The finding that the NFD–PHPA solid dispersions exhibit two T_gs has also supported the partial immiscibility between NFD and PHPA.[14] T_gs at 46°C and 70°C for the NFD–PHPA (30%) solid dispersions may correspond to the T_g of amorphous NFD alone and that of the NFD–PHPA matrix, respectively. NFD may be present in a supersaturated state, and may be more sensitive to the physical stimulation of tapping than amorphous NFD without polymer or with PEG.

CONCLUSIONS

Atomic force microscopy was found to be a useful tool for studying the crystallization kinetics of amorphous solids by targeting crystals at the surface. The ability to obtain three-dimensional information at the surface is one of the advantages of AFM, as well as its nanoscale resolution, enabling it to detect minute topographical changes that can indicate the crystal growth rate in a short time. However, two phenomena revealed in this study need to be borne in mind when interpreting the data obtained by AFM measurements: (1) Although crystal structures are captured at the surface of the sample by AFM, the crystal formation may not always be initiated at the surface. The change in surface topography may reflect the growth of crystals from the bulk. (2) Physical stimulation by the AFM probe may affect the crystallization rate, as shown for NFD crystallization in NFD–PHPA solid dispersions.

ACKNOWLEDGMENTS

Part of this work was supported by a grant-in-aid for Research on Publicly Essential Drugs and Medical Devices from The Japan Health Sciences Foundation.

REFERENCES

1. Bunjes H, Rades T. 2005. Thermotropic liquid crystalline drugs. J Pharm Pharmacol 57:807–816.
2. Murdande SB, Pikal MJ, Shanker RM, Bogner RH. 2001. Solubility advantage of amorphous pharmaceuticals: I. A thermodynamic analysis. J Pharm Sci 99:1254–1264.
3. Blagden N, de Matas M, Gavan PT, York P. 2007. Crystal engineering of active pharmaceutical ingredients to improve solubility and dissolution rates. Adv Drug Deliv Rev 59:617–630.
4. Wu T, Yu L. 2006. Surface crystallization of indomethacin below T_g. Pharm Res 23:2350–2355.
5. Zhu L, Wong L, Yu L. 2008. Surface-enhanced crystallization of amorphous nifedipine. Mol Pharm 5:921–926.
6. Liao X, Wiedmann TS. 2006. Formation of cholesterol crystals at a mucin coated substrate. Pharm Res 23:2413–2416.
7. Cassidy AM, Gardner CE, Jones W. 2009. Following the surface response of caffeine cocrystals to controlled humidity storage by atomic force microscopy. Int J Pharm 379:59–66.
8. Price R, Young PM. 2004. Visualization of the crystallization of lactose from the amorphous state. J Pharm Sci 93:155–164.
9. Mahlin D, Berggren J, Alderborn G, Engström S. 2004. Moisture-induced surface crystallization of spray-dried amorphous lactose particles studied by atomic force microscopy. J Pharm Sci 93:29–37.
10. Mahlin D, Berggren J, Gelius U, Engström S, Alderborn G. 2006. The influence of PVP incorporation on moisture-induced surface crystallization of amorphous spray-dried lactose particles. Int J Pharm 321:78–85.
11. Chan KL, Kazarian SG. 2004. FTIR spectroscopic imaging of dissolution of a solid dispersion of nifedipine in poly(ethylene glycol). Mol Pharm 1:331–335.

12. Vippagunta SR, Wang Z, Hornung S, Krill SL. 2007. Factors affecting the formation of eutectic solid dispersions and their dissolution behavior. J Pharm Sci 96:294–304.
13. Bley H, Fussnegger B, Bodmeier R. 2010. Characterization and stability of solid dispersions based on PEG/polymer blends. Int J Pharm 390:165–173.
14. Aso Y, Yoshioka S, Miyazaki T, Kawanishi T, Tanaka K, Kitamura S, Takakura A, Hayashi T, Muranushi N. 2007. Miscibility of nifedipine and hydrophilic polymers as measured by ^{1}H-NMR spin-lattice relaxation. Chem Pharm Bull 55:1227–1231.
15. Rumondor AC, Marsac PJ, Stanford LA, Taylor LS. 2009. Phase behavior of poly(vinylpyrrolidone) containing amorphous solid dispersions in the presence of moisture. Mol Pharm 6:1492–1505.
16. Giammona G, Carlisi B, Plazzo S. 1987. Reaction of α,β-poly(N-hydroxyethyl)-DL-aspartamide with derivatives of carboxylic acids. J Polym Sci Polym Chem Ed 25:2813–2818.

 DOI 10.1002/jps

Netsu Sokutei **38** (4) 125-131

解　説

熱分析による非晶質医薬品の結晶化の評価

宮崎 玉樹，阿曽 幸男

（受取日：2011年6月23日，受理日：2011年7月29日）

Evaluation of Crystallization of Amorphous Drugs by Thermal Analysis

Tamaki Miyazaki and Yukio Aso

(Received June 23, 2011; Accepted July 29, 2011)

About half of candidates for active pharmaceutical ingredients are poorly water soluble compounds. Amorphization of poorly water soluble drugs has attracted much attention due to improved dissolution characteristics and bioavailability of amorphous drugs. On the other hand, crystallization during storage is of concern for amorphous drugs. Therefore, evaluation of crystallization of amorphous drug is important for developing stable pharmaceuticals using amorphous drugs. In this article, feasibility of thermal method such as differential scanning calorimeter and isothermal microcalorimeter for evaluating crystallization of amorphous drugs and research topics on the crystallization of amorphous drug are described.
Keywords; amorphous, crystallization, DSC, isothermal microcalorimetry,

1. はじめに

近年の医薬品開発における候補化合物の選択は、標的分子との親和性を指標に行われるため，候補化合物の半数は水に溶けにくいと言われている。このような候補化合物を医薬品として上市するためには，製剤化に際して溶解性を改善するための工夫が必要となる。溶解性の改善のためには可溶性の塩，可溶性のプロドラッグへの変換やシクロデキストリン等との複合体形成など化学的な変換を行うアプローチや，有機溶媒や界面活性剤による可溶化などが考えられる。これらの方法は候補化合物の特性により適用が限られる場合があり，使用可能な有機溶媒や界面活性剤の制限もある。一方，準安定形への結晶化，微粒子化，非晶質化など，候補化合物の物理的状態を変化させることにより溶解性を改善する方法もある。これらの方法は候補化合物を高いエネルギー状態にすることにより溶解性を改善するものであり，適用できる化合物の適用範囲が比較的広く，多くの候補化合物において研究が行われている。しかし，このような物理的なアプローチは，準安定形結晶においては安定形結晶への転移，微粒子化においては凝集や粒子サイズの増大，非晶質化においては結晶化など，安定な状態へ変化する可能性があることが問題点である。このような変化は医薬品の有効性や安全性に影響を及ぼす可能性があるため，医薬品開発においてはこのような変化が起こるかどうか，また，起こるのであればどのようなタイムスケールで起こるのかなどを評価することは非常に重要なことである。我々は物理的なアプローチのなかでも安定状態への変化の可能性が大きいと考えられる非晶質化による溶解性の改善に注目し，ジヒドロピリジン系の医薬品やフェノバルビタールなどをモデルとし，結晶化の速度論的な解析や結晶化に及ぼす温度，湿度，高分子添加剤などの影響について研究を行っている。

本解説においては示差走査熱量測定（DSC）や等温ミクロ熱量測定（IMC）などの熱分析による非晶質医薬品の結晶化の評価の有用性について述べる。

2. DSCによる非晶質薬物の結晶化の評価

非晶質薬物のDSCのデータは非晶質薬物の結晶化を評価するうえで有用な情報を与える。**Fig.1**に非晶質ニフェジピン，ニトレンジピンおよびニルバジピンのDSCの測定例を示す。非晶質固体はある温度においてガラス状態から過冷却液体へ転移し（ガラス転移），それに伴い試料の比熱が変

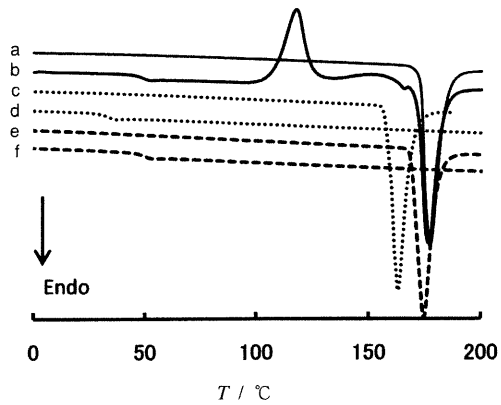

Fig.1 Typical DSC traces for crystalline and amorphous nifedipine (**a**, **b**), nitrendipine (**c**, **d**) and nilvadipine (**e**, **f**).

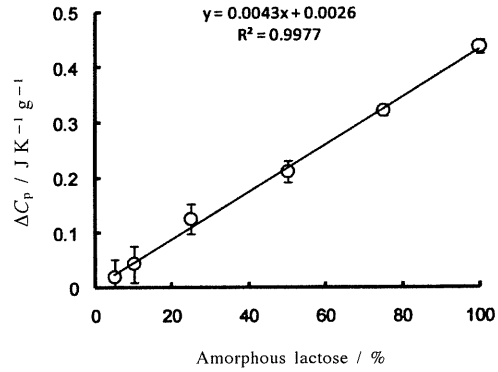

Fig.2 Calibration curve for amorphous lactose in the physical mixture of freeze-dried lactose and lactose hydrate.

化する。**Fig.1(b),(d),(f)**のトレースに示されるように非晶質ニフェジピン，ニルバジピンでは50℃付近に，非晶質ニトレンジピンでは30℃付近にガラス転移に伴うベースラインの断絶が観測された。また，非晶質ニフェジピンにおいては120℃付近にDSCの昇温過程における結晶化にともなう発熱ピークが見られたが，非晶質ニトレンジピンやニルバジピンにおいてはDSCの昇温過程における結晶化に伴う発熱ピークが見られなかった。これらの結果から，ニフェジピンに比べニトレンジピンやニルバジピンは結晶化しにくいと考えることができ，DSCの昇温中における結晶化の有無によって結晶化のしやすさを定性的に評価できる。結晶化のしやすさをより定量的に評価するためには，非晶質薬物の残存量が時間とともにどのように変化するかを明らかにする必要がある。試料中の非晶質薬物の残存量はガラス転移温度（T_g）における比熱の変化量（ΔC_p），結晶化熱（ΔH_c）および融解熱（ΔH_m）を指標に見積もることができる。ただし，ΔH_cを指標として用いる場合にはDSCの昇温過程において，残存する非晶質薬物が定量的に結晶化する必要がある。また，ΔH_mを指標として用いるためにはDSCの昇温過程において結晶化が進行しないことが必要である。非晶質ニフェジピンは**Fig.1(b)**に示すようにDSCの昇温過程において結晶化し，非晶質ニフェジピンの残存量の指標としてΔC_pまたはΔH_cを使用できる。両者の指標を用いることにより同様のタイムコースを得ることができた。ニトレンジピンの調製直後の非晶質試料は**Fig.1(d)**に示すように昇温過程において結晶化しない。しかし，保存後のニトレンジピンの試料においては2つの融解ピークが観測され，2つの融解ピークの比率は試料間でバラツキが見られたため，ΔH_mを指標として用いることはできなかった。そこで，3つの薬物に共通に適用できるΔC_pを用いて，以下の検討を行った。ΔC_pが非晶質薬物の残存量の指標として使用できることを確認するために，**Fig.2**に凍結乾燥によって調製した非晶質乳糖と乳糖水和物の物理混合物についてΔC_pを測定した結果を示す。観測されたΔC_pの値は物理混合物中の非晶質乳糖の比率との間に良好な直線関係が得られた。**Fig.3**に種々の非晶質薬物について測定した非晶質薬物の残存率と保存時間の関係を示す。[1-3] 保存前の試料について得られる$\Delta C_p(0)$とt時間保存した試料の$\Delta C_p(t)$の比から，保存試料中の非晶質薬物の残存率$R(t)$を算出しプロットした。

$$R(t) = \Delta C_p(t) / \Delta C_p(0) \qquad (1)$$

クローズドシンボルは60℃で保存したニフェジピン（T_g＝41℃），ニトレンジピン（T_g＝27℃），ニルバジピン（T_g＝43℃）の結果であり，他のシンボルは45℃で保存したニフェジピン，フェノバルビタール（T_g＝37℃），フロプロピオン（T_g＝55℃)およびアセトアミノフェン（T_g＝25℃)の結果を示す。また，図に示す曲線はAvrami式(式(2))にフィットして得られたものである。

$$R(t) = \exp\{-kt^n\} \qquad (2)$$

ここで，nは結晶化のメカニズムに依存する定数であり，薬物によって異なる。**Fig.3**の非晶質薬物の残存率のタイムコースから示されるように結晶化のしやすさは薬物によって大きく異なった。T_gが高い薬物ほど結晶化しにくい傾向が見られるが，例外も見られる。例えば，ニフェジピン（T_g＝41℃）とニルバジピン（T_g＝43℃）を比較すると，ほぼ同様のT_gにもかかわらず，ニルバジピンの結晶化は非常に遅かった。また，ニルバジピンにくらべフロプロピオン（T_g＝55℃）のT_gは高いが，45℃で保存したフロプロピオ

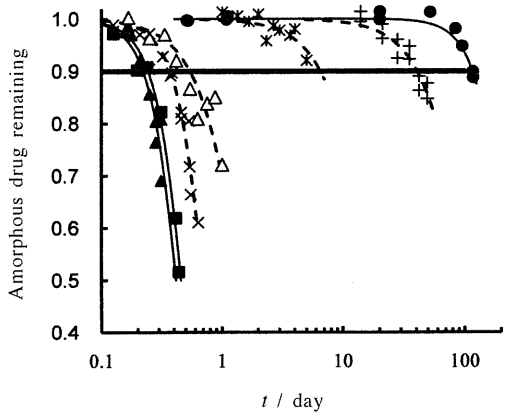

Fig.3 Typical time courses for crystallization of amorphous drugs stored at 60 (closed symbol) or 45 ℃.
▲, nifedipine, 60 ℃; ■, nitrendipine, 60 ℃; ●, nilvadipine, 60 ℃; △, nifedipine, 45 ℃; ＊, phenobarbital, 45 ℃; +, flopropine, 45 ℃; ×, acetaminophen, 45 ℃.

ンは，60 ℃で保存したニルバジピンより速やかに結晶化が進行した。T_gは非晶質薬物の結晶化のしやすさの指標になるが，T_g以外の因子も結晶化のしやすさに関与していることを示唆する結果と考えられる。従って，結晶化速度に影響を及ぼす因子を明らかにすることは，非常に興味深いことと考える。

以下の議論においては非晶質薬物の残存率が0.9になる時間t_{90}を結晶化のしやすさの指標として用いる。結晶化のしやすさに影響を及ぼす因子を考察するために，類似のジヒドロピリジン環構造を有するニフェジピン，ニトレンジピン，ニルバジピンについて，t_{90}に及ぼす温度，湿度の影響を検討し，その結果を**Fig.4**に示す。オープンシンボルは乾燥状態の試料について得られた結果である。ニルバジピンとニトレンジピンは温度が低いほどt_{90}が長くなり，結晶化が起こりにくくなる。それに対し，ニフェジピン（□）のt_{90}の温度依存性はT_g（$1000/T=3.1$）付近で断絶が見られた。Ishidaらによってもニフェジピンの結晶成長速度の温度依存性にT_g付近で断絶があることが報告されている。Ishidaらは検討した温度範囲において生成する結晶形が同じであることから，結晶成長速度の温度依存性のT_g付近における断絶は結晶化メカニズムがT_g付近で変化すると考えており，T_g以上の温度においては拡散が律速（diffusion controlled）のメカニズムにより結晶化するのに対し，T_g以下の温度ではNon-diffusion controlledメカニズムによって起こると考えている。[4]

Fig.4のクローズドシンボルは非晶質ニルバジピンを一定

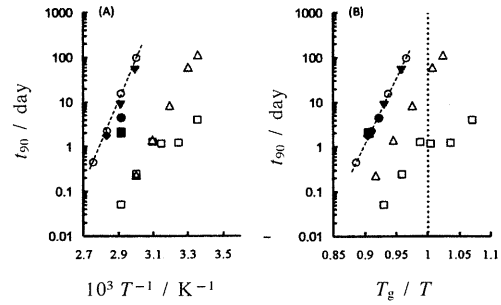

Fig.4 Temperature dependence of t_{90} for amorphous nifedipine (□), nitrendipine (△) and nilvadipine (○, ◆, ■, ●, ▼).
Relative humidity: □, △, ○, 0%; ◆, 11%; ▼, 23%; ●, 56%; ◆, 75%.

の相対湿度に保存し，吸湿させた試料について得られた結果を示す。保存湿度が高く，吸湿量が多いと考えられる試料ほどt_{90}が短かった。また，吸湿させた試料のT_gは保存湿度が高い試料ほど低かった。結晶化は核生成と結晶成長の2つの過程によって進行し，これらの過程の速度の温度依存性は分子運動性の因子（＝粘度）と熱力学的な因子（＝結晶と非晶質の自由エネルギーの差に起因する因子と結晶化によって新たな界面が生成することによる自由エネルギーの増えに起因する因子）によって支配されると報告されている。[5] **Fig.4(B)**に示すように，吸湿によるT_gの低下を考慮し，t_{90}の値をT_g/Tに対してプロットすると，ニルバジピンのt_{90}のデータは1つの直線上に集まった。T_gの変化は試料の粘度（＝分子運動性）の変化を反映することから，試料の吸湿は主に分子運動性を変化させ，結晶化のしやすさに影響していると考えられる。吸湿による分子運動性の変化が結晶のしやすさに影響することはニトレンジピンやニフェジピンにおいても観察されている。[3] しかし，高分子が共存する場合には水は分子運動性に影響を及ぼす他に，高分子とともに溶媒として作用し，過飽和度に影響することが報告されている。[6] 水の結晶化に及ぼす影響についてさらに検討する必要があると考えられる。

ニフェジピン，ニトレンジピン，ニルバジピンはジヒドロピリジン環を有し，類似の化学構造をもつが，ニルバジピンのt_{90}の値は他の2つの薬物のt_{90}の値と大きく異なった。分子運動性の因子（$=T_g$）の影響を除くためにT_g/Tに対してプロットしても薬物間のt_{90}の違いは見られ，熱力学的因子が薬物間のt_{90}の差をもたらしているものと考えられる。結晶と非晶質の自由エネルギーの差（ΔG_v）はHoffman式（式(3)）によって見積もることができる。[7]

$$\Delta G_v = \{\Delta H_m \times (T_m - T) \times T\}/T_m^2 \qquad (3)$$

Table 1 Thermodynamic parameters of amorphous drugs.

Drug	ΔGv at T_g J m^{-3}	T_g / ℃	T_m / ℃	ΔH_m / kJ mol^{-1}
Nifedipine	3.13 ×10^7	41.3 ±0.2	172.5 ±0.5	37.9 ±0.8
Nitrendipine	3.07 ×10^7	27.1 ±0.4	156.0 ±0.6	39.0 ±0.5
Nilvadipine	2.77 ×10^7	42.8. ±0.4	168.1 ±0.4	39.1 ±0.7

ここで，ΔH_m，T_mは融解熱と融点を表す。

Table 1に示すように，T_gにおける単位体積当たりのΔG_vの値はニフェジピン>ニトレンジピン>ニルバジピンの順である。従って，**Fig.4(B)**に示すT_gにおける結晶化のしやすさの順と同じであり，結晶と非晶質の自由エネルギーの差が非晶質医薬品の安定性の差に一部寄与していると考えられる。しかし，ΔG_vの違いのみで安定性の差を説明するためにはその差が小さく，界面自由エネルギーの寄与や結晶化メカニズムの違いも関与していると考えられる。

ポリビニルピロリドン（PVP）やヒドロキシプロピルメチルセルロース（HPMC）などの水溶性高分子添加剤は非晶質薬物の結晶化を抑制することが知られている。結晶化の抑制は，薬物に比べ高いT_gを有する高分子添加剤を添加することにより，薬物単独に比べT_gが上昇し，分子運動性が抑制されるためであると言われている。また，T_gの変化の見られないような少量の高分子の添加によっても結晶化が抑制されることから，薬物と高分子の相互作用も結晶化抑制に寄与していると考えられる。薬物－高分子相互作用の結晶化速度に及ぼす影響を検討するために，分子運動性に差がないと考えられるニトレンジピンエナンチオマーを用い，セルロース誘導体を添加した固体分散体中の結晶化速度を明らかにした。[8] ニトレンジピンは不斉炭素を有し，光学活性カラム（CHIRALCEL OJ-H，ダイセル化学工業(株)）を用いたHPLCにより光学分割を行うことができる。230 nmの紫外光に対する円偏光二色性の符号に基づきHPLCにおいて先に溶出するエナンチオマーを(-)-ニトレンジピン，後から溶出するものを(+)-ニトレンジピンと記す。得られたそれぞれのエナンチオマーのT_g，T_mなどの物理化学特性は同一であった。**Fig.5**に結晶化のタイムコースを示す。薬物単独の場合はエナンチオマー間で結晶化のタイムコースに差は見られなかった。また，不斉炭素を有するがランダムな立体配置をとっているため光学活性を有しないPVPを添加した場合もエナンチオマー間で結晶化のタイムコースに差は見られなかった。それに対し，セルロース由

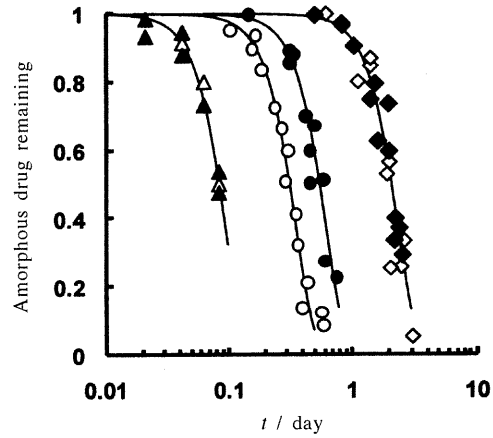

Fig.5 Time courses of crystallization of (+)-nitrenndipine (closed symbols) and (-)-nitrendipine (open symbols) in the absence (△, ▲) and presence of 10%PVP (◇, ◆) or 10%HPMC(○, ●) at 60℃.

Table 2 t_{90} for crystallization of nitrendipine enantiomers.

T / ℃	Polymer	t_{90} / h (-)-nitrendipine	(+)-nitrendipine
40	None	41	41
	10% HPMC	235	230
50	None	5.7	5.7
	10% PVP	250	250
	10% HPMC	17	25
60	None	1.1	1.1
	10% PVP	25	25
	10% HPMC	3.9	6.8

来であり，光学活性を有するHPMCを添加した固体分散体においては(+)-ニトレンジピンは(-)-ニトレンジピンに比べ結晶化が遅いことが示された。このエナンチオマー間の安定性の差は相互作用の差によるものと考えられる。ニトレンジピンの結晶化のt_{90}値を**Table 2**に示す。50℃や60℃においては，HPMCを添加した(+)-ニトレンジピンは(-)-ニトレンジピンに比べ1.5倍程度t_{90}が長く，HPMCは(+)-ニトレンジピンをより安定化するが，40℃においては，エナンチオマー間でt_{90}に差が見られなかった。その理由を十分に説明することはできないが，以下のような説明が可能かもしれない。結晶化速度の温度依存性は，先に述べたように分子運動性の因子と熱力学的な因子によって支配されるが，T_g付近やそれより低い温度領域では分子運動性の因子が支配的であると言われている。HPMCを添加したニト

Table 3 Cohesive energy density of nitrendipine enantiomers at 25 ℃.

polymer	Cohesive energy density / $\times 10^8$ J m^{-3}	
	(S)-nitrendipine	(R)-nitrendipine
None	5.36	5.37
PVP	5.00	4.93
HPMC	5.56	5.58

レンジピンのT_gはエナンチオマー間で差がなく（(+)-ニトレンジピン-10 % HPMC: 33.0 ± 0.7 ℃，(-)-ニトレンジピン-10 % HPMC: 33.1 ± 1.0 ℃），分子運動性にエナンチオマー間で差がない。従って，40 ℃においてはエナンチオマー間でt_{90}に差が見られなかったものと考えられる。

薬物-高分子相互作用の検出は赤外吸収スペクトルによって行われることが多いが，HPMCを添加したニトレンジピンの赤外吸収スペクトルはエナンチオマー間で大きな差が見られなかった。そこで，分子動力学的シミュレーションによる凝集エネルギーを指標として，相互作用の差を検出できるか検討した。凝集エネルギーは，セル中に存在する原子1つ1つをそれぞれ無限大の距離に引き離すために必要なエネルギーを表わし，高分子間の相互作用の大きさにエナンチオマー間で差があれば凝集エネルギーに反映されるとの仮定に基づいている。ニトレンジピンエナンチオマーとPVPまたはHPMCの混合物のモデルをMaterials Studioソフトウェア（Accelrys）のAmorphousCellモジュールを用いて作成した。混合物のモデルはニトレンジピンエナンチオマー20分子とモノマーユニット数が10の高分子3分子を用いた(薬物と高分子の重量比　約1:1)。Discoverモジュールを用いて分子動力学シュミュレーションを行い，凝集エネルギーを算出した。力場はpcffを用いた。25 ℃でエネルギー極小化処理を行った後，圧力一定条件下で5,000ステップの平衡化を行った。次に，平衡化されたセルについて体積一定条件下で100,000 ～ 2,000,000ステップの動力学計算を行い，原子の座標の軌跡を数フレーム得た。得られたフレームについて凝集エネルギーを算出した。**Table 3**に示すように凝集エネルギーはエナンチオマー間で差は見られなかった。t_{90}のエナンチオマー間の差は1.5倍程度であり，HPMCとニトレンジピンエナンチオマー間の相互作用の差は赤外吸収スペクトルや凝集エネルギーには反映されないような小さな差であると考えられる。

3. IMCによる非晶質薬物の結晶化の評価

IMCは，DSCに比べ高い精度で温度制御が可能であり（± 10^{-6} K），ノイズが少なく，安定なベースラインが得られるため，DSCに比べ高感度な測定が可能である。従って，

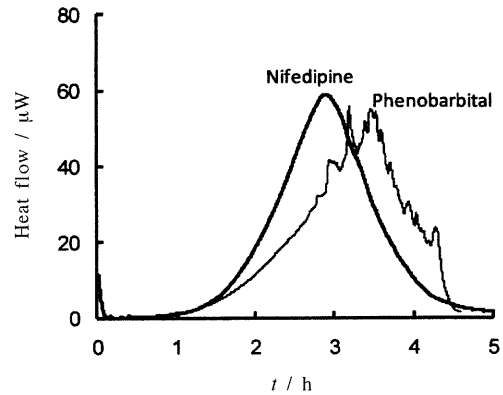

Fig.6 Typical heat flow-time curves of amorphous nifedipine and phenobaribital at 65 ℃.

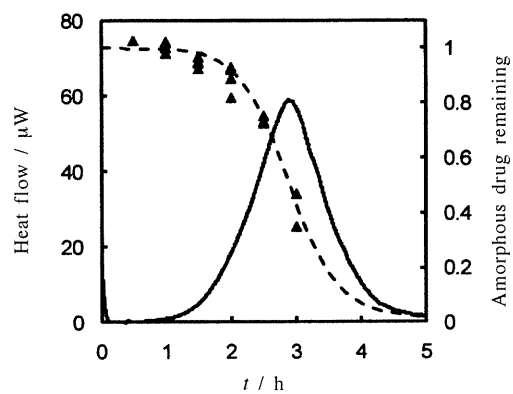

Fig.7 Comparison of amorphous nifedipine remaining estimated from IMC (---) and DSC (▲).

結晶化の進行が緩やかな温度条件においても，結晶化に伴う発熱を経時的に測定することが可能であり，非晶質医薬品の結晶化の過程を直接的に観測できる。[9] **Fig.6**に非晶質ニフェジピン，フェノバルビタールの測定例を示す。いずれの薬物も3から4時間後に発熱のピークが観測された。Heat flowが0に戻った試料についてDSCの測定を行うと結晶ニフェジピンあるいは結晶フェノバルビタールの融解による吸熱ピークが観測された。このことから，**Fig.6**に示されるHeat flowは非晶質ニフェジピンあるいはフェノバルビタールの結晶化に基づく発熱であることが分かる。全体のHeat flow curveを積分して得られる熱量（H）と時間tまでのHeat flowの積分値（H_t）との比（H_t/H）は結晶化の進行度x_tを表し，$1-x_t$を計算することにより試料に残存する非晶質薬物の残存率が得られる。IMCのHeat flow

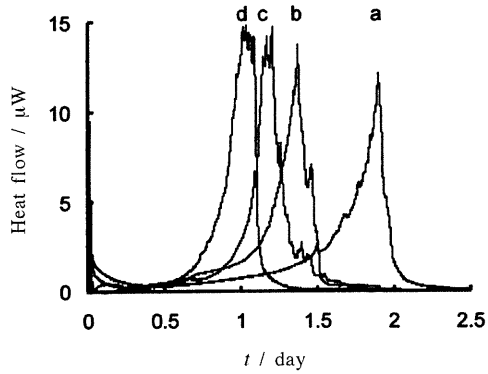

Fig.8 Effect of relative humidity in the ample on heat flow-time curve of amorphous nifedipine at 50 ℃.
Relative humidity: b, 22%; c, 40%; d, 56%.
a: ample was purged by dry nitrogen before the ample was closed.

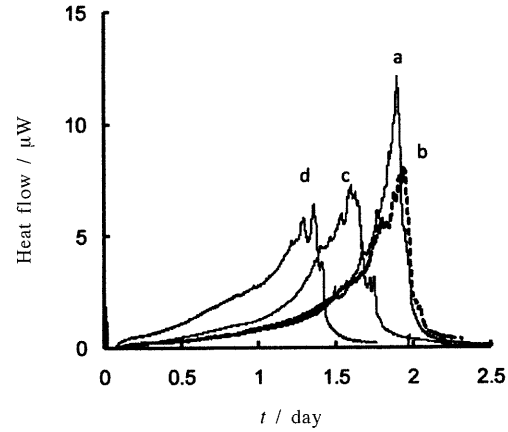

Fig.9 Effect of thermal history on heat flow-time curve of amorphous nifedipine at 50 ℃.
a, initial; b, -20 ℃ for 17 months; c, 5 ℃ for 40 days; d, 25 ℃ for 2days.

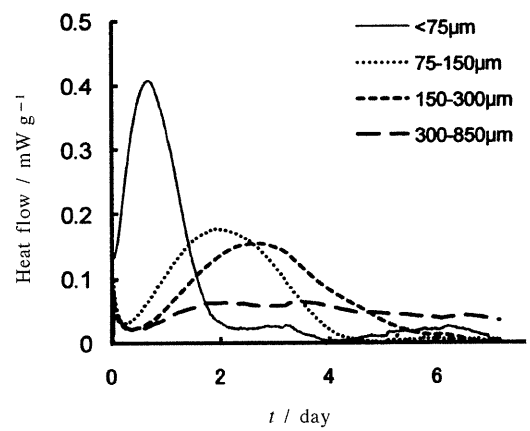

Fig.10 Effect of particle size on heat flow-time curve of amorphous nifedipine at 25 ℃.

から算出した残存率を**Fig.7**に示す。破線で示されるIMCから得られた非晶質薬物の残存率は，別途，T_gにおける比熱の変化量をもとに算出した残存率（▲)のタイムコースとほぼ一致した。

IMCでは1つの試料で結晶化のタイムコースが得られるため，さまざまな因子が結晶化速度に及ぼす影響を比較的簡便に明らかにできる。例えば，測定前に種々の湿度に1時間保存したアンプルに非晶質ニフェジピンを入れ，そのHeat flowを測定すると，**Fig.8**に示すように，保存湿度が高いほど発熱のピーク到達時間が短く，結晶化が速やかに進行していることが分かる。これは，アンプル内の水分がニフェジピンのT_gを低下させ，その結果，分子運動性が高まり，結晶化が促進されたものと考えられる。このように，結晶化速度に及ぼす水分の影響を比較的簡便に評価することができる。また，結晶化速度に及ぼす熱履歴の影響もIMCのHeat flowのタイムコースから明らかにできる。**Fig.9**に種々の温度条件で保存した非晶質ニフェジピンのHeat flowの測定例を示す。5 ℃で40日あるいは25 ℃で2日保存した試料では，発熱のピーク到達時間が調製直後の試料に比べ短かった。これは，IMC測定前の保存の間に結晶核の生成などの非晶質マトリックスの変化が起こり，結晶化に伴う発熱が観測されるまでのラグタイムが短くなった結果と考えられる。−20 ℃で17か月保存したサンプルは調製直後の試料と同様のタイムコースが得られ，非晶質マトリックスの変化は起こらなかったものと考えられる。

最近，非晶質固体の表面における結晶成長は非晶質固体の内部における結晶成長比べ1オーダー以上速やかに進行することが報告されている。[10,11] 非晶質医薬品の表面の結晶化は溶解性へ影響を及ぼすと予想され，非晶質固体の表面と内部の安定性の違いを評価し，溶解性の改善に対する表面の結晶化のインパクトを理解することは安定な非晶質医薬品を開発する上で非常に重要である。IMCはこのような非晶質固体の表面と内部の安定性の違いの評価に有用であると考えられる。**Fig.10**は粒子サイズを変えて表面と内部の比率を変化させた非晶質ニフェジピンのHeat flow曲線を示す。試料の粉砕，ふるい分け，試料のIMC用のアンプルへの封入は乾燥窒素中で行い，4つの試料は同時に測定したものである。粒子サイズの小さな試料ほど短時間で発熱が観測された。IMC測定後にDSCの測定を行った結果，